

Online DNN-driven Nonlinear MPC for Stylistic Humanoid Robot Walking with Step Adjustment

Giulio Romualdi^{†,1}, Paolo Maria Viceconte^{†,1}, Lorenzo Moretti¹, Ines Sorrentino^{1,2},
Stefano Dafarra¹, Silvio Traversaro¹ and Daniele Pucci^{1,2}

Abstract—This paper presents a three-layered architecture that enables stylistic locomotion with online contact location adjustment. Our method combines an autoregressive Deep Neural Network (DNN) acting as a *trajectory generation* layer with a model-based *trajectory adjustment* and *trajectory control* layers. The DNN produces centroidal and postural references serving as an initial guess and regularizer for the other layers. Being the DNN trained on human motion capture data, the resulting robot motion exhibits locomotion patterns, resembling a human walking style. The trajectory adjustment layer utilizes non-linear optimization to ensure dynamically feasible center of mass (CoM) motion while addressing step adjustments. We compare two implementations of the trajectory adjustment layer: one as a receding horizon planner (RHP) and the other as a model predictive controller (MPC). To enhance MPC performance, we introduce a Kalman filter to reduce measurement noise. The filter parameters are automatically tuned with a Genetic Algorithm. Experimental results on the ergoCub humanoid robot demonstrate the system’s ability to prevent falls, replicate human walking styles, and withstand disturbances up to 68 Newton.

I. INTRODUCTION

Designing trajectories for humanoid robots involves addressing complex interactions between high-dimensional multi-body systems and the environment. Additionally, in scenarios where unexpected disturbances affect the robot, it becomes essential to adapt the planned contact position to prevent falls. There are two fundamental approaches to control humanoid robot locomotion: *data-driven* and *model-based*. The data-driven approach involves designing a reinforcement learning infrastructure that takes high-level commands and the robot’s state as input, generating joint references. This architecture produces natural robot motions [1], [2], but it suffers from the sim-to-real gap [3]. On the other hand, the model-based approach usually involves a hierarchical architecture with three main layers [4]. Each layer generates references for the inner layers by processing inputs from the robot, the environment, and the outer layers. From top to bottom, these layers are referred to as *trajectory generation*, *trajectory adjustment*, and *trajectory control*.

This paper aims to bridge the gap between the data-driven and the model-based approaches, proposing a hierarchical control architecture where a Deep Neural Network (DNN) acts as a trajectory generation layer and a Model Predictive

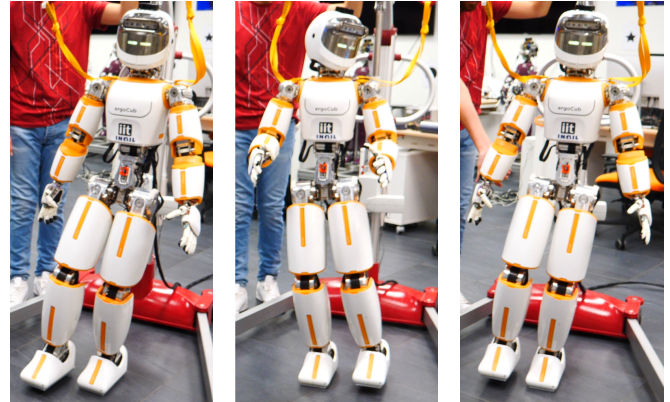


Fig. 1: The humanoid robot ergoCub walks forward, sideways, and reacts to an external force with the proposed locomotion architecture.

Control (MPC) serves as a trajectory adjustment layer. This infrastructure enables stylistic human-like locomotion with online step adjustment capabilities.

Within the model-based architecture, the *trajectory generation* layer is responsible for computing a sequence of contact locations and timings, along with joint and center of mass (CoM) trajectories. This layer can be designed using *model-based* or *learning-based* methods. In the model-based approach, optimization techniques are applied to evaluate the feasibility of contact locations, utilizing both whole-body robot models [5] or template models [6], [7]. While providing enhanced planning capabilities, a whole-body trajectory generator may lead to extended computation time [8], preventing their use in real-time. Predefined contact locations and timings allow whole-body planners to operate in real-time [9]; however, in case of external disturbances, the contact position is not adapted. Instead, limiting the robot CoM height and the angular momentum during walking simplifies the robot model into template models, making the problem treatable online [6], [10]. However, these architectures tend to neglect stylistic properties of the generated motions, as they are challenging to explicitly encode and optimize for [11], [12]. On the other hand, learning-based approaches leverage data-driven techniques to transfer stylistic locomotion patterns to the robot. These methods often utilize human motion capture (MoCap) data to train DNNs [13], [14].

The *trajectory adjustment* layer considers the output of the trajectory generation layer and the robot state to adjust contact locations and the CoM trajectory. This layer often relies on template models that consider a constant [15], [16] or adaptive [17], [18] step duration. However, simplified model-

[†] Paolo Maria Viceconte and Giulio Romualdi are co-first authors.

¹ Artificial and Mechanical Intelligence, Istituto Italiano di Tecnologia, Genoa, Italy name.surname@iit.it

² School of Computer Science, University of Manchester, Manchester, United Kingdom

This paper was supported by the Italian National Institute for Insurance against Accidents at Work (INAIL) ergoCub Project.

based controller architectures often treat footstep adjustment separately from the primary control loop [19], [20]. An alternative approach involves framing the problem as a whole-body MPC and solving it using differential dynamic programming (DDP) [21]. Given the complexity of the problem, it is necessary to correctly warm-start the DDP algorithm to obtain reliable results [22]. Conversely, one can model the robot as a single rigid body [23] or consider its centroidal dynamics [24] to deal with the step adjustment within the main control loop [25], [26].

Finally, the *trajectory control* layer generates robot commands to stabilize the references produced by its preceding layers. This layer considers whole-body kinematics or dynamics. The associated optimization problem is typically structured with either strict or weighted stack of task [15], [27] and framed as a Quadratic Programming (QP) problem.

This paper presents a solution for online whole-body trajectory generation within a model-based control framework by leveraging data-driven methods. Specifically, the DNN extracts references from MoCap data to initialize the trajectory-adjustment layer. This architecture enables stylistic-human-like locomotion patterns with online step adjustment capabilities. In detail, our contributions are: i) An architecture that connects a DNN trajectory generator with a MPC-based trajectory adjustment layer. This approach is demonstrated using Mode-Adaptive Neural Networks (MANN) [28] as DNN. ii) A MPC formulation ensuring kinematically-feasible motions of the robot's CoM while addressing step adjustment. Unlike previous approaches [26], [29], our proposed controller uses a control-barrier function to ensure that the CoM remains within a safe region. iii) Benchmarking of two implementations of trajectory adjustment layer acting as a Receding Horizon Planner (RHP) and as a MPC, respectively. In the latter case, we introduce a Kalman filter (KF) [30] to reduce the noise of CoM velocity and angular momentum measurements. KF parameters are optimized via a genetic algorithm (GA). The system is validated on the position-controlled humanoid robot ergoCub – Fig. 1. We demonstrate the effectiveness of the proposed architecture in preventing the robot from falling while walking, when subject to impulsive disturbances up to 68 N. The style of the robot motion echoes the MoCap data.

The paper is organized as follows. Sec.II introduces notation and background. Sec.III presents the layers of the proposed architecture and their interconnection. Sec.IV shows the results and their discussion. Sec.V concludes the paper.

II. BACKGROUND

A. Notation

- I_n and 0_n represent $n \times n$ identity and zero matrices;
- e_i indicates the canonical base, i.e., $e_3^\top = [0 \ 0 \ 1]$
- \mathcal{I} denotes the inertial frame;
- ${}^A p_C$ is a vector that connects the origin of frame \mathcal{A} and the origin of frame \mathcal{C} expressed in the frame \mathcal{A} ;
- Given ${}^A p_C$ and ${}^B p_C$, ${}^A p_C = {}^A R_B {}^B p_C + {}^A p_B = {}^A H_B {}^B p_C$, where ${}^A H_B$ is the homogeneous transformation and ${}^A R_B \in SO(3)$ is the rotation matrix;

- the *hat operator* is $\wedge : \mathbb{R}^3 \rightarrow \mathfrak{so}(3)$, such that $x \wedge y = x \times y$. \times is the cross product operator in \mathbb{R}^3 ;
- ${}^A v_B \in \mathbb{R}^3$ is the time derivative of the relative position between the origin of the frame \mathcal{B} and \mathcal{A} , ${}^A v_B = {}^A \dot{p}_B$;
- ${}^A f_B \in \mathbb{R}^3$ is the force acting on \mathcal{B} expressed in \mathcal{A} ;
- for the sake of clarity, the prescript \mathcal{I} will be omitted.

B. Centroidal dynamics

The centroidal momentum $\bar{c}h^\top = \begin{bmatrix} \bar{c}h^{p^\top} & \bar{c}h^{\omega^\top} \end{bmatrix} \in \mathbb{R}^6$ is the combined linear and angular momentum of each robot link, relative to the robot's CoM [24]. The vectors $\bar{c}h^p \in \mathbb{R}^3$ and $\bar{c}h^\omega \in \mathbb{R}^3$ denote the linear and angular momentum, respectively. The coordinates of $\bar{c}h$ are expressed with respect to a frame centered at the robot's CoM and oriented as \mathcal{I} [24]. In the case of rectangular contact surfaces the time derivative of the centroidal momentum writes as

$$\bar{c}\dot{h} = \sum_{i=1}^{n_c} \sum_{j=1}^4 \begin{bmatrix} I_3 \\ (H_{p_{C_i}} p_{v_{i,j}} - p_{\text{CoM}})^\wedge \end{bmatrix} f_{i,j} + \begin{bmatrix} mg \\ 0_{3 \times 1} \end{bmatrix}. \quad (1)$$

Where m is the robot's mass, n_c is the number of active contacts. $p_{v_{i,j}}$ is the position of vertex j of contact i , expressed with respect to the frame associated with the contact surface. $H_{p_{C_i}}$ is the pose of the contact i . $f_{i,j} \in \mathbb{R}^3$ denotes the pure force applied to vertex j of contact i .

C. Control Barrier Function

Let us consider a discrete dynamical system $x_{k+1} = f(x_k, u_k)$ where $x_k \in X \subseteq \mathbb{R}^n$ is the system state and $u_k \in U$ is the control input. We define a *safe set* $\Omega = \{x \in X : g(x) \geq 0\}$ as the superlevel set of a continuously-differentiable function $g : X \subseteq \mathbb{R}^n \rightarrow \mathbb{R}$. g is a discrete-time control barrier function (CBF) [31] if satisfies

$$\Delta g(x_{k+1}, x_k) \geq -\gamma g(x_k), \quad (2)$$

where $\Delta g(x_{k+1}, x_k) = g(x_{k+1}) - g(x_k)$, with $0 < \gamma \leq 1$.

D. Problem statement

Let us consider the architecture in Fig. 2, where an autoregressive DNN generates trajectories and a MPC adjusts them dynamically. The goal is to seamlessly integrate these layers, allowing the MPC to use the DNN-generated trajectories as a warm start, despite their potential lack of dynamic feasibility [28]. This integration faces several challenges:

- \mathcal{C}_1 : the DNN-based trajectory generation lacks contact awareness, whereas the MPC needs contact locations and timings.
- \mathcal{C}_2 : the DNN provides next-instant outputs, but the MPC needs a trajectory over a time horizon.
- \mathcal{C}_3 : the DNN is trained with a dataset collected at a specific frequency, while the MPC may expect references at a different rate.

These challenges are addressed by designing ad-hoc blocks to extract contact information, generate trajectories for the time horizon, and match reference frequencies, respectively, as detailed in Sec. III-E.

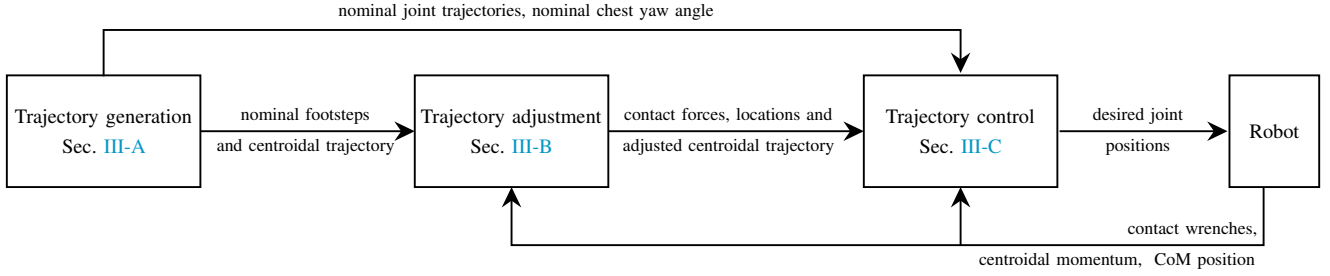


Fig. 2: The proposed three-layer hierarchical architecture integrating a DNN as a trajectory generation layer and a model-based trajectory adjustment layer.

III. LOCOMOTION ARCHITECTURE

This section illustrates the main components of the architecture presented in Fig. 2 and their interconnection.

A. Trajectory Generation

Given a high-level target motion to be followed, the objective of the trajectory generation layer is to generate the associated footstep plan, joint positions, and centroidal trajectory. The generation problem is framed as a nonlinear autoregressive model, trained on human MoCap data and fed at inference time with its own output, conditioned by the high-level target provided by an external user. The choice of the DNN architecture, the data processing, and the real-time inference follow [28] and are summarized hereafter.

1) *Network architecture*: We adopt as DNN the MANN architecture [32], which is characterized by a Motion Prediction Network and a Gating Network. The former predicts the next trajectory data point given the previous one. The latter predicts the blending coefficients which are used at inference time to compute the weights of the Motion Prediction Network as a linear combination of K learnable experts.

2) *Data processing*: The DNN is trained on tailored features extracted from MoCap data [28] retargeted onto the robot model using the Whole-Body Geometric Retargeting method [33] for the joint positions. To prevent the stance foot from sliding, the base orientation is directly retrieved from the human data, while the base position is computed by forward kinematics, using the lowest foot vertex as the fixed contact point. Differently from [28], we constrain the shoulder roll retargeting to prevent self-collisions. Each network input includes the motion of the base projected on the ground and retargeted joint positions and velocities. Outputs consist of subsequent base trajectory and joint configuration.

3) *Real-time inference*: During inference, the input from the external user is collected through a joystick. This user-defined base trajectory is combined with the one generated by the network. Alongside the predicted joint configuration, this merged base trajectory becomes the input for the network in the next iteration. This interactive process empowers the user to actively influence and guide the trajectory generation.

B. Trajectory Adjustment

The trajectory adjustment layer aims to compute feasible contact wrenches and locations while taking into account the centroidal dynamics and the output of the trajectory generation layer. Similarly to [29], the control objective is formulated

here as a MPC consisting of three fundamental components: the *prediction model*, an *objective function*, and a collection of *inequality constraints*.

1) *Prediction Model*: We introduce a variable $\Gamma_i \in \{0, 1\}$ to represent the contact state for a given time instant t . $\Gamma_i(t) = 0$ if the contact i is not active at t , $\Gamma_i(t) = 1$ otherwise. Consequently, we rewrite (1) as

$$\bar{G}\dot{h} = \sum_{i=1}^2 \sum_{j=1}^4 \begin{bmatrix} I_3 \\ (H_{p_{C_i}} p_{v_{i,j}} - p_{CoM})^\wedge \end{bmatrix} \Gamma_i f_{i,j} + \begin{bmatrix} mg \\ 0_{3 \times 1} \end{bmatrix}. \quad (3)$$

To ensure that the MPC efficiently computes real-time control outputs, we design the optimal control problem in a way that remains agnostic to the number of active contact phases within the prediction horizon. This is accomplished by considering each contact location p_{C_i} as a continuous variable evolving with the following dynamics:

$$\dot{p}_{C_i} = (1 - \Sigma_i) v_{C_i}, \quad (4)$$

where v_{C_i} is a slack variable, and $\Sigma_i \in \{0, 1\}$ is related to Γ_i as follows. When $\Gamma_i = 1$, Σ_i must also be 1. However, $\Gamma_i = 0$ does not necessarily imply $\Sigma_i = 0$. When $\Sigma_i = 1$ then $\dot{p}_{C_i} = 0$, meaning that the contact position remains constant. The introduction of this additional parameter prevents contact adjustment when the contact is about to be established, differently from [29].

2) *Objective Function*: The objective function consists of multiple tasks that together stabilize the dynamics (3).

a) *Centroidal trajectory tracking*: To ensure that the robot follows a desired centroidal momentum trajectory, we minimize the error between the robot's angular momentum and CoM trajectories with respect to the nominal as

$$\Psi_h = \left\| \bar{G}h^{\omega^n} - \bar{G}h^{\omega} \right\|_{\Lambda_h}^2 + \left\| p_{CoM}^n - p_{CoM} \right\|_{\Lambda_{CoM}}^2, \quad (5)$$

where Λ_h and Λ_{CoM} are positive definite diagonal matrices.

b) *Contact location regularization*: To prevent the controller from computing adjusted contact locations too far from the nominal $p_{C_i}^n$, we introduce the following term:

$$\Psi_{p_{C_i}} = \left\| p_{C_i}^n - p_{C_i} \right\|_{\Lambda_{p_{C_i}}}^2, \quad (6)$$

where $\Lambda_{p_{C_i}}$ is a positive definite diagonal matrix.

c) *Contact force regularization*: To ensure that the four contact forces acting on each foot remain similar between each other and continuous, we introduce the following tasks:

$$\Psi_{f_{i,j}} = \left\| \frac{f_i}{n_v} - f_{i,j} \right\|_{\Lambda_{f_{i,j}}}^2 + \left\| e_3^\top (f_i^n - f_i) \right\|_{\Lambda_{f_i}}^2 + \left\| \dot{f}_{i,j} \right\|_{\Lambda_{\dot{f}_{i,j}}}^2. \quad (7)$$

Here $\Lambda_{\dot{f}_{i,j}}$, $\Lambda_{f_{i,j}}$ and Λ_{f_i} are positive definite diagonal matrices. f_i is the sum of all contact forces applied to the corners for contact i , while f_i^n denotes the nominal contact force computed heuristically. The x and y components of the nominal force are always set to zero. The z component depends on the contact's status. When the robot is in single support, this component equals the robot's weight on the contact foot and is zero on the other one. In double support, it is interpolated using a first-order spline. In (7), the first term penalizes the difference between the forces at different corners, the second regularizes the force to a predefined value, and the last term reduces the force rate of change.

3) *Inequality constraints*: Several inequality constraints concur to generate feasible MPC outputs.

a) *CoM height limit*: Differently from [29], we introduce a CBF to ensure that the height of the CoM remains within a safe region, $\Omega \in [p_{\text{CoM}_z}^{\min}, p_{\text{CoM}_z}^{\max}]$. For each time instant t , we define the following CBF:

$$g(t) = -\alpha(p_{\text{CoM}_z}^{\min} - p_{\text{CoM}_z})(p_{\text{CoM}_z}^{\max} - p_{\text{CoM}_z}), \quad (8)$$

where $\alpha > 0$, and p_{CoM_z} is the z-coordinate of the CoM. Eq. (8) is then used to define a set of nonlinear inequality constraints of the form (2).

b) *Contact Force Feasibility*: To be considered feasible, the contact force must belong to the friction cone [34], which is here approximated using a conic combination of n vectors. This approximation is represented as a set of linear inequalities, $AR_{C_i}^\top f_{i,j} \leq b$, where A and b are constants determined by the static friction coefficient.

c) *Contact location constraint*: To satisfy the robot's kinematic limits, we ask for the contact location to be inside a l_b by w_b rectangle centered on the nominal contact position and oriented as the nominal foot. This is expressed by:

$$l_b \leq R_{C_i}^\top (p_{C_i}^n - p_{C_i}) \leq w_b. \quad (9)$$

4) *MPC formulation*: We tackle the MPC problem by integrating the prediction model (Sec. III-B.1), the objective function (Sec. III-B.2), and the inequality constraints (Sec. III-B.3). We employ the Direct Multiple Shooting method with a constant sampling time T_{MPC} [35]. The controller generates outputs using the Receding Horizon Principle [36], with a fixed N -samples prediction window.

5) *MPC and receding horizon planner*: The formulation presented in Sec. III-B.4 computes the contact locations and forces. For a torque-controlled robot, the desired contact forces can be directly set in the trajectory control layer. If the robot's available control mode is position control, the trajectory adjustment layer can be integrated in two ways: as a RHP or as a proper MPC. In the RHP setting, the contact forces are integrated using the centroidal dynamics (1). The

resulting CoM position is provided as input to the inner layer and fed back to the planner. This method completely decouples the trajectory adjustment block from the robot, making the layer function as a planner. Conversely, in the MPC setting, the trajectory adjustment layer receives feedback from the robot, specifically the current CoM position, velocity, and angular momentum. The predicted CoM quantities are then used as input to the inner layer, allowing the trajectory adjustment layer to close the loop with the robot state.

C. Trajectory Control

The trajectory control layer generates the joint references to the robot and it consists of three main components: a CoM-ZMP controller, a swing foot planner, and a QP-inverse kinematics (IK).

1) *CoM-ZMP controller*: The CoM-ZMP controller guarantees the tracking of the desired zero moment point (ZMP) [37] by using the control law [4]

$$\dot{p}_G^* = \dot{p}_G^{\text{ref}} - K_{\text{ZMP}}(x_{\text{ZMP}}^{\text{ref}} - x_{\text{ZMP}}) + K_G(p_G^{\text{ref}} - p_G). \quad (10)$$

Here, p_G^{ref} and p_G denote the reference and measured ground-projected CoM, whereas $x_{\text{ZMP}}^{\text{ref}}$ and x_{ZMP} refer to the reference and measured ZMP.

2) *Swing foot planner*: Given a footstep list, we employ a minimum acceleration planner to generate the swing foot trajectory, as in [4].

3) *QP-IK*: The joint trajectories are computed by framing the controller as a constrained optimization problem. As in [4], low-priority tasks are integrated into the cost function, high-priority tasks become constraints, and the robot velocity is the optimization variable. In our formulation, the high-priority tasks include the feet poses and CoM tracking. Additionally, we introduce regularizations for the joint positions and chest orientation as low-priority tasks. We formulate the IK as a QP problem and solve it using off-the-shelf solvers. Once the joint velocity is calculated, it is integrated and sent to the robot's low-level position control.

D. Joint Velocity estimation

When the trajectory adjustment layer acts as a MPC, reducing the noise in the estimated joints velocity is crucial to obtain smoother measurements of the CoM velocity and the angular momentum. To accomplish this, we estimate the joints velocity using a KF with the following system dynamics

$$\begin{bmatrix} s_{k+1} \\ \dot{s}_{k+1} \\ \ddot{s}_{k+1} \end{bmatrix} = \begin{bmatrix} 1 & T & 0 \\ 0 & 1 & T \\ 0 & 0 & 1 \end{bmatrix} \begin{bmatrix} s_k \\ \dot{s}_k \\ \ddot{s}_k \end{bmatrix} + v. \quad (11)$$

T is the sampling time, and $v \sim \mathcal{N}(0, Q)$ is the process noise. The measurement equation is $y_k = s_k + w$, where $w \sim \mathcal{N}(0, R)$. The covariance state at $t = 0$ is $P_0 = \lambda I_3$.

To reduce the need for manual hand-tuning, we identify the KF covariance matrices by maximizing an objective function:

$$\xi^* = \arg \max_{\xi} \mathcal{G}(\xi). \quad (12)$$

$\xi \in \mathbb{R}_+^5$ is the vector containing the initial state covariance parameter $\lambda \in \mathbb{R}_+$, the diagonal terms of the covariance

matrix $Q \in \mathbb{R}^{3 \times 3}$, and the value of the measurement covariance $R \in \mathbb{R}_+$. To compute ξ , we collect a joint position dataset and, for each point, compute the estimated output of the KF along with the following objective function $\mathcal{G}_i(\xi)$:

$$\mathcal{G}_i(\xi) = -(w_j \dot{s}_i^2 + w_a \ddot{s}_i^2 + (s_i - \hat{s}_i)^2 + (s_i - \hat{s}_i^v)^2 + (s_i - \hat{s}_i^a)^2). \quad (13)$$

Here, w_a and w_j are positive weights, and $\hat{(\cdot)}$ indicates the quantities estimated by the KF. \hat{s}_i^v and \hat{s}_i^a are the joint positions numerically integrated from the estimated velocity and acceleration, respectively. In (13), the first two terms encourage the continuity of the estimated quantities by minimizing the jerk and the acceleration, while the last three terms drive the KF to estimate velocity and acceleration such that their integration does not drift from the position. The objective function $\mathcal{G}(\xi)$ in (12) is computed as the sum of the objective functions for each timestep and optimized using GA.

E. System integration

This section addresses the challenges introduced in Sec. II-D and further describes the interconnections between the layers of our architecture in Fig. 2.

1) \mathcal{C}_1 : The main objective of the trajectory generation layer is to compute the *nominal* CoM, angular momentum, and footsteps used in the MPC objective function — Eqs. (5), (6), (7). However, the autoregressive DNN described in Sec. III-A predicts only the joint states and the base pose. So, we compute the centroidal quantities by applying the forward kinematics. The contact states are inferred through a Schmitt trigger. When a corner of the foot is below a given threshold for a predefined amount of time, we consider the contact active. We then determine the contact location through forward kinematics, zeroing the height of the foot. As the length of the generated footsteps may require torques that closely approach the joint torque limits, we iteratively scale the generated footsteps and CoM positions as follows:

$$p_{\circ_i}^s = p_{\circ_{i-1}}^s + \gamma(p_{\circ_i}^n - p_{\circ_{i-1}}^n). \quad (14)$$

Here, p_{\circ} represents either the contact or the CoM position. The indices i and $i-1$ correspond to two consecutive time steps for the CoM or two consecutive footsteps in the case of contacts. The superscripts s and n denote the scaled and nominal quantities, respectively. The parameter $\gamma > 0$ is the scaling factor. Similarly, the centroidal trajectory and contact timings are time-scaled by a positive factor η . The higher η , the slower the trajectory.

2) \mathcal{C}_2 : The DNN computes the output for the next time step, but the trajectory adjustment layer requires a trajectory over an entire horizon. To bridge this gap, the DNN inference is executed iteratively, generating a trajectory that matches the duration specified by the MPC’s horizon while keeping the joystick input constant – Sec. III-A.3. Since the DNN might be trained with a dataset collected at a different frequency than the MPC, we need to synchronize the calls of the trajectory generation and adjustment layers. To address this, we generate trajectories for the MPC horizon in a separate process at a rate δ_{DNN} determined by the least common multiple of

the MPC sampling time, T_{MPC} , and the scaled DNN period, ηT_{DNN} . This approach minimizes the frequency of trajectory generator calls, improving the system’s overall performance. The network outputs are stored for the entire horizon, and the sample at index $\delta_{\text{DNN}}/\eta T_{\text{DNN}}$ is used to reset the DNN when a new trajectory is required.

3) \mathcal{C}_3 : To provide to the MPC references at its expected rate, we resample the generated trajectories at the MPC sampling time using a first-order spline.

4) *Interconnections*: As regards the interconnection between the trajectory generation and adjustment layer, we initialize the latter with nominal values of CoM, angular momentum, and contact locations provided by the former. Depending on whether the trajectory adjustment layer functions as a MPC or a RHP, its feedback varies. For the MPC, the feedback is the robot state. For the RHP, the feedback consists of the previously-integrated desired centroidal quantities. To make the RHP aware of external disturbances affecting the robot, the measured external wrench is used as a disturbance in the prediction model – Eq. (3)

Regarding the interconnection between the trajectory adjustment and control layers, we feed the adjusted footstep list produced by the former to the swing foot planner. The planner can update the foot trajectory with new desired contact positions even during the swinging phase. Moreover, the desired CoM for the CoM-ZMP controller (10) is obtained from the MPC’s predicted state when the trajectory adjustment layer acts as a controller, or integrated from computed contact forces when it acts as RHP. The desired ZMP is computed from the desired contact forces provided by the trajectory adjustment layer. Finally, the trajectory generation layer is directly connected to the trajectory control layer to provide the nominal joint trajectories which serve as a regularizer in the QP-IK problem.

IV. RESULTS

In this section, we present the validation results for the architecture discussed in Sec. III. Our implementation of MANN features a Motion Prediction Network and a Gating Network, each with 3 hidden layers of 512 and 32 units, respectively, using $K = 4$ experts. We consider $n = 26$ joints. Human MoCap data is collected using an Xsens suit [38], containing 17 inertial sensors. The data includes 20 minutes of walking motions and transitions on flat terrain at $T_{\text{DNN}} = 20$ ms, resulting in 150k training points when mirrored. The network, implemented in PyTorch [39] and trained using AdamWR [40] for 110 epochs, takes about 7 hours on an NVIDIA GeForce GTX 1650 GPU for training. Online inference uses ONNX Runtime [41]. For the non-linear MPC optimization problem, we use CasADi 3.6.2 [42] and IPOPT 3.14.12 [43] with HSL_MA97 [44] libraries. The IK-QP problem in the trajectory control layer is solved with osqp-eigen and the OSQP library [45]. Kalman Filter gains are optimized using a GA with PyGAD [46], running for 50 generations with 60 parents selected for mating. The population size is 120, using k -tournament selection ($k = 4$) and a two-point crossover strategy. A 20% per gene mutation

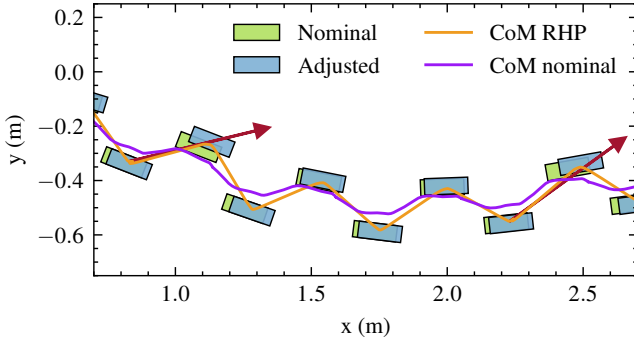


Fig. 3: Top-view of the walking pattern performed by ergoCub with the trajectory adjustment layer acting as RHP. The robot is pushed twice. The red arrows represent the external pushes.

rate with random mutations is used, preserving the top 10% of solutions in each generation. Data for the GA consist of a 6-minute trajectory sampled at 1 kHz, for a total of about 360k points. Optimizing the values for all 26 controlled joints takes around 7 hours, averaging 30 minutes per joint, on an AMD EPYC 7513 32-core Processor. The architecture is implemented in C++ and the code is available at <https://sites.google.com/view/dnn-mpc-walking>.

To validate the performance of the proposed architecture, we conduct two main experiments involving forward walking and turning. In the first experiment, the trajectory adjustment layer operates as a RHP, while in the second one, it functions as a MPC. Both experiments, shown in the accompanying video, are conducted on the 160 cm tall, 56 kg ergoCub humanoid robot. The architecture runs on a 10th-generation Intel Core i7-10750H laptop running Ubuntu Linux 22.04.

A. Trajectory Adjustment layer as RHP

In this experiment, the trajectory adjustment layer operates with a sampling time $T_{MPC} = 60$ ms and 1.2 s horizon. The trajectory control runs at 500 Hz. The nominal footsteps are scaled by $\gamma = 0.7$ and $\eta = 3$, resulting in $\delta_{DNN} = 60$ ms.

Fig. 3 shows the nominal and adjusted footsteps, the nominal CoM, and the CoM computed from the integration of the RHP output. The nominal CoM, used as a warm start for the RHP, undergoes significant modifications to meet force feasibility constraints and the objective function in Sec. III-B. Moreover, since the step adjustment is always considered in the RHP formulation, the nominal footsteps are continuously modified. A more pronounced step adjustment emerges when the robot is perturbed with an external impulsive force applied to its right arm during walking, as indicated by the red arrows in Fig. 3. Being the trajectory adjustment layer implemented as a RHP, it is not aware of CoM perturbances. To address this, we incorporate the estimated external force as a measured disturbance in the centroidal dynamics in Eq. (3) as well as in the contact forces integrator of Sec. III-B.5. Given the impulsive nature of the external force, we consider the disturbance to be non-zero only for the first sample of the RHP horizon, setting it to zero for the remaining window. The external force is estimated online considering the readouts of the Force Torque sensors mounted on the robot arms and the robot state [47]. The RHP compensates for the disturbance

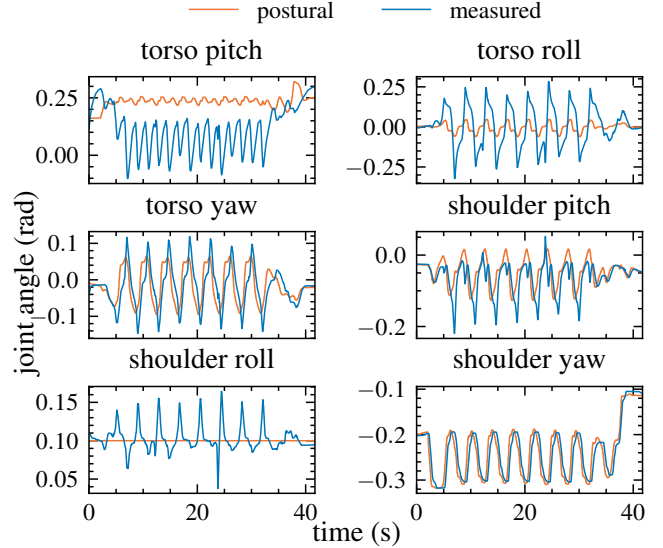


Fig. 4: Measured upper body joint angles - specifically, torso and left arm - compared with their associated data-driven postural during walking.

effect by adjusting the footstep locations up to 5 cm under a 63 N impulsive force.

In Fig. 4, we examine how closely the measured joint positions follow their associated data-driven posturals. The upper body joints display periodic patterns similar to human data, unlike traditional humanoid locomotion architectures that use a fixed postural reference [28]. As the QP-IK incorporates a task to zero the chest roll and pitch angles, the measured values for the torso joints exhibit larger deviations from their associated postural compared to the other joints. The shoulder roll postural remains constant because of the retargeting constraint to prevent self-collisions. Overall, the upper body motion contributes to shaping the robot’s movement to resemble human MoCap data, as shown in the accompanying video.

B. Trajectory Adjustment layer as MPC

When the trajectory adjustment layer implements a closed-loop MPC, it is necessary to reduce the MPC sampling time to $T_{MPC} = 50$ ms to achieve smoother and faster reactions to external disturbances, while the trajectory control operates at 500 Hz. As before, the MPC time horizon is 1.2 s. In this experiment, the nominal footsteps are scaled by factors $\gamma = 0.6$ and $\eta = 3$, respectively, therefore $\delta_{DNN} = 300$ ms.

The top plot of Fig. 5 represents the nominal and adjusted footsteps, the nominal and predicted CoM. As in the previous experiment, the nominal CoM, which serves as a warm start for the MPC, undergoes significant modifications to meet the force feasibility constraints and optimize the objective function. With the trajectory adjustment layer implemented as a MPC, it now adjusts the contact foot positions based on the CoM state. Three external disturbances, labeled A, B, and C, affect the system. Each disturbance impacts the robot’s arm, which behaves compliantly. During disturbance A, the robot experiences a push on its shoulder. Since only the shoulder is compliant and reaches its joint limit, the change in the

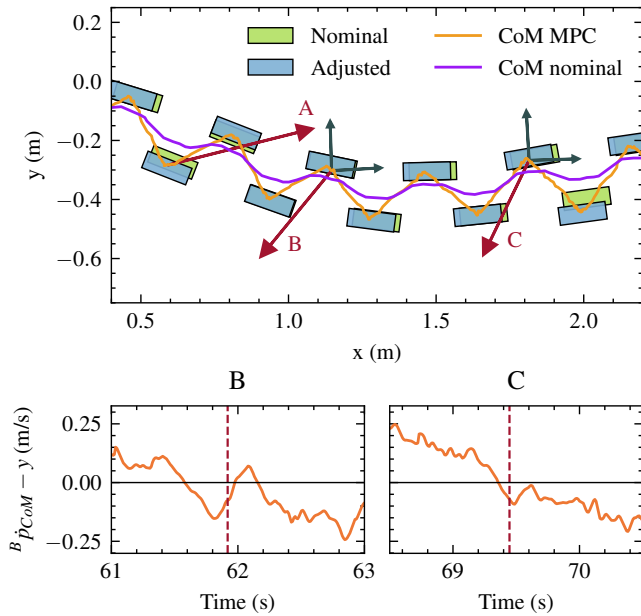


Fig. 5: Top-view of the walking pattern performed by ergoCub with the trajectory adjustment layer functioning as a model predictive controller MPC. The robot is pushed three times, as indicated by the red arrows. For the second (B) and third (C) disturbances, occurring at 61.9 s and 69.43 s respectively, the lateral (local y -coordinate) CoM velocity is displayed. The red dashed line marks the time at which the system is perturbed.

CoM is limited, resulting in a small footstep adjustment. In contrast, disturbances B and C involve pulling forces on the robot. Although the pulling forces in B and C are comparable (about 68 N), step recovery is triggered only after C. This difference arises because the MPC is integrated within a three-layer architecture, where also the trajectory control layer can adjust the CoM trajectory at a higher frequency to prevent the robot from falling. In scenario B, the step adjustment is not triggered because the body CoM velocity ${}^B\dot{p}_{\text{CoM}}$ on the lateral plane at $t \approx 61.90$ s is positive, i.e. opposite to the external disturbance on the y coordinate, indicating that the robot is not falling. Conversely, in scenario C, the body CoM velocity ${}^B\dot{p}_{\text{CoM}}$ on the lateral plane at $t \approx 69.43$ s is negative, i.e. aligned with the external disturbance, suggesting that the robot is about to fall inward. Therefore, the step recovery is automatically triggered.

In Fig. 6, we present the values of the objective function (13) for several joints of the left leg across different GA iterations. The plot demonstrates that, after approximately 20 iterations, the objective function values converge to their maximum, indicating successful optimization. Similar convergence behavior is observed for the other joints as well.

C. RHP vs MPC

The experiments in Sec. IV-A and Sec. IV-B reveal different behaviors when the trajectory adjustment layer functions as a RHP or as a MPC. In the case of RHP, since the feedback is derived from desired quantities, the layer is unaffected by measurement noise, allowing for longer steps. However, to prevent falls from external pushes, RHP must explicitly consider external disturbances, requiring reliable force measurements. Conversely, with MPC, no force measurements are needed as

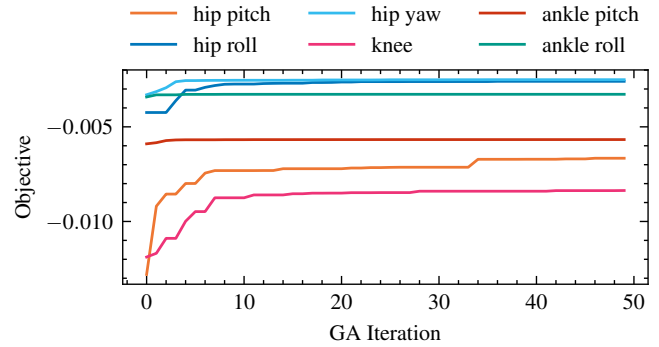


Fig. 6: Values of the objective function across GA iterations for the KF parameters estimation of the left leg.

it uses the robot’s kinematic state as feedback. This feedback can be noisy due to joint velocity estimation errors, necessitating extensive tuning. Our GA-tuned KF mitigates this issue, making the trajectory adjustment acting as MPC the best compromise for a complete integrated locomotion architecture.

V. CONCLUSION

This paper contributes towards bridging the gap between model-based trajectory adjustment and data-driven trajectory generation for humanoid robot locomotion. The trajectory adjustment layer implements a MPC or a RHP and ensures dynamically-feasible CoM motion while addressing the step adjustment problem. The two implementations are benchmarked. In the case of MPC, we introduced a GA-tuned KF to reduce joint velocity noise and consequently CoM velocity and angular momentum noise. Results on the ergoCub humanoid robot indicate that the architecture prevents falls, replicates human MoCap walking styles, and withstands disturbances up to 68 N.

The current system lacks a base estimator, limiting its ability to handle stronger pushes. Adding a base estimator would improve fall detection and consequently contact position adjustment. Transitioning to torque control would also enhance natural responses to disturbances. Future work will focus on integrating a base estimator and torque control to improve robustness and enable handling more significant perturbations.

REFERENCES

- [1] I. Radosavovic, T. Xiao, B. Zhang, T. Darrell, J. Malik, and K. Sreenath, “Real-World Humanoid Locomotion with Reinforcement Learning,” 3 2023.
- [2] Z. Li, X. B. Peng, P. Abbeel, S. Levine, G. Berseth, and K. Sreenath, “Reinforcement Learning for Versatile, Dynamic, and Robust Bipedal Locomotion Control,” 1 2024.
- [3] D. Kim, G. Berseth, M. Schwartz, and J. Park, “Torque-Based Deep Reinforcement Learning for Task-and-Robot Agnostic Learning on Bipedal Robots Using Sim-to-Real Transfer,” *IEEE Robotics and Automation Letters*, vol. 8, no. 10, pp. 6251–6258, 10 2023.
- [4] G. Romualdi, S. Dafarra, Y. Hu, P. Ramadoss, F. J. A. Chavez, S. Traversaro, and D. Pucci, “A Benchmarking of DCM-Based Architectures for Position, Velocity and Torque-Controlled Humanoid Robots,” *International Journal of Humanoid Robotics*, vol. 17, no. 01, p. 1950034, 2 2020.
- [5] H. Dai, A. Valenzuela, and R. Tedrake, “Whole-body motion planning with centroidal dynamics and full kinematics,” in *2014 IEEE-RAS International Conference on Humanoid Robots*, vol. 2015-Febru, IEEE, 2015, pp. 295–302.

- [6] T. Takenaka, T. Matsumoto, and T. Yoshiike, "Real time motion generation and control for biped robot -1;supçstj/supç report: Walking gait pattern generation-," in *2009 IEEE/RSJ International Conference on Intelligent Robots and Systems*. IEEE, 10 2009, pp. 1084–1091.
- [7] J. Engelsberger, C. Ott, and A. Albu-Schaffer, "Three-Dimensional Bipedal Walking Control Based on Divergent Component of Motion," *IEEE Transactions on Robotics*, vol. 31, no. 2, pp. 355–368, 4 2015.
- [8] Q. Nguyen, X. Da, J. W. Grizzle, and K. Sreenath, "Dynamic Walking on Stepping Stones with Gait Library and Control Barrier Functions," 2020, pp. 384–399.
- [9] E. Dantec, M. Taix, and N. Mansard, "First Order Approximation of Model Predictive Control Solutions for High Frequency Feedback," *IEEE Robotics and Automation Letters*, vol. 7, no. 2, pp. 4448–4455, 4 2022.
- [10] J. Engelsberger, G. Mesesan, C. Ott, and A. Albu-Schaffer, "DCM-Based Gait Generation for Walking on Moving Support Surfaces," in *2018 IEEE-RAS 18th International Conference on Humanoid Robots (Humanoids)*. IEEE, 11 2018, pp. 1–8.
- [11] E. Hsu, K. Pulli, and J. Popović, "Style translation for human motion," *ACM Transactions on Graphics*, vol. 24, no. 3, pp. 1082–1089, 7 2005.
- [12] H. Du, E. Herrmann, J. Sprenger, K. Fischer, and P. Slusallek, "Stylistic Locomotion Modeling and Synthesis using Variational Generative Models," in *Motion, Interaction and Games*. New York, NY, USA: ACM, 10 2019, pp. 1–10.
- [13] K. Bergamin, S. Clavet, D. Holden, and J. R. Forbes, "DRCon: data-driven responsive control of physics-based characters," *ACM Transactions on Graphics*, 2019.
- [14] S. Starke, I. Mason, and T. Komura, "DeepPhase: periodic autoencoders for learning motion phase manifolds," *ACM Transactions on Graphics*, vol. 41, no. 4, pp. 136:1–136:13, 2022.
- [15] B. J. Stephens and C. G. Atkeson, "Push Recovery by stepping for humanoid robots with force controlled joints," in *2010 10th IEEE-RAS International Conference on Humanoid Robots*. IEEE, 12 2010, pp. 52–59.
- [16] M. Shafiee, G. Romualdi, S. Daffarra, F. J. A. Chavez, and D. Pucci, "Online dcm trajectory generation for push recovery of torque-controlled humanoid robots," *IEEE-RAS International Conference on Humanoid Robots*, vol. 2019-October, pp. 671–678, 10 2019.
- [17] R. J. Griffin, G. Wiedebach, S. Bertrand, A. Leonessa, and J. Pratt, "Walking stabilization using step timing and location adjustment on the humanoid robot, Atlas," *IEEE International Conference on Intelligent Robots and Systems*, vol. 2017-September, pp. 667–673, 12 2017.
- [18] N. Scianca, D. De Simone, L. Lanari, and G. Oriolo, "MPC for Humanoid Gait Generation: Stability and Feasibility," *IEEE Transactions on Robotics*, vol. 36, no. 4, pp. 1171–1188, 8 2020.
- [19] M.-J. Kim, D. Lim, G. Park, and J. Park, "Foot Stepping Algorithm of Humanoids with Double Support Time Adjustment based on Capture Point Control," in *2023 IEEE International Conference on Robotics and Automation (ICRA)*. IEEE, 5 2023, pp. 12 198–12 204.
- [20] A. Dallard, M. Benallegue, N. Scianca, F. Kanehiro, and A. Kheddar, "Robust Bipedal Walking with Closed-Loop MPC: Adios Stabilizers," 2024.
- [21] J. Shim, C. Mastalli, T. Corbères, S. Tonneau, V. Ivan, and S. Vijayakumar, "Topology-Based MPC for Automatic Footstep Placement and Contact Surface Selection," in *2023 IEEE International Conference on Robotics and Automation (ICRA)*. IEEE, 5 2023, pp. 12 226–12 232.
- [22] E. Dantec, R. Budhiraja, A. Roig, T. Lembono, G. Saurel, O. Stasse, P. Fernbach, S. Tonneau, S. Vijayakumar, S. Calinon, M. Taix, and N. Mansard, "Whole Body Model Predictive Control with a Memory of Motion: Experiments on a Torque-Controlled Talos," in *2021 IEEE International Conference on Robotics and Automation (ICRA)*. IEEE, 5 2021, pp. 8202–8208.
- [23] R. Grandia, A. J. Taylor, A. D. Ames, and M. Hutter, "Multi-Layered Safety for Legged Robots via Control Barrier Functions and Model Predictive Control," in *2021 IEEE International Conference on Robotics and Automation (ICRA)*. IEEE, 5 2021, pp. 8352–8358.
- [24] D. Orin, A. Goswami, and S.-H. Lee, "Centroidal dynamics of a humanoid robot," *Autonomous Robots*, 2013.
- [25] Y. Ding, C. Khazoom, M. Chignoli, and S. Kim, "Orientation-Aware Model Predictive Control with Footstep Adaptation for Dynamic Humanoid Walking," in *2022 IEEE-RAS 21st International Conference on Humanoid Robots (Humanoids)*. IEEE, 11 2022, pp. 299–305.
- [26] X. Meng, Z. Yu, X. Chen, Z. Huang, F. Meng, and Q. Huang, "Online Adaptive Motion Generation for Humanoid Locomotion on Non-Flat Terrain via Template Behavior Extension," *IEEE Transactions on Automation Science and Engineering*, pp. 1–12, 2024.
- [27] S. Caron, A. Kheddar, and O. Tempier, "Stair Climbing Stabilization of the HRP-4 Humanoid Robot using Whole-body Admittance Control," in *2019 International Conference on Robotics and Automation (ICRA)*. IEEE, 5 2019, pp. 277–283.
- [28] P. M. Viceconte, R. Camoriano, G. Romualdi, D. Ferigo, S. Daffarra, S. Traversaro, G. Oriolo, L. Rosasco, and D. Pucci, "ADHERENT: Learning Human-like Trajectory Generators for Whole-body Control of Humanoid Robots," *IEEE Robotics and Automation Letters*, vol. 7, no. 2, pp. 2779–2786, 4 2022.
- [29] G. Romualdi, S. Daffarra, G. L'Erario, I. Sorrentino, S. Traversaro, and D. Pucci, "Online Non-linear Centroidal MPC for Humanoid Robot Locomotion with Step Adjustment," in *2022 International Conference on Robotics and Automation (ICRA)*. IEEE, 5 2022, pp. 10 412–10 419.
- [30] R. E. Kalman, "A New Approach to Linear Filtering and Prediction Problems," *Journal of Basic Engineering*, vol. 82, no. 1, pp. 35–45, 3 1960.
- [31] Y. Sun, D. Wu, L. Gao, Y. Gao, Y. Pan, and N. Ding, "Safety-Critical Control and Path Following by Formations of Agents with Control Barrier Functions using Distributed Model Predictive Control," in *2023 35th Chinese Control and Decision Conference (CCDC)*. IEEE, 5 2023, pp. 1818–1823.
- [32] H. Zhang, S. Starke, T. Komura, and J. Saito, "Mode-adaptive Neural Networks for Quadruped Motion Control," *ACM Transactions on Graphics*, 2018.
- [33] K. Darvish, Y. Tirupachuri, G. Romualdi, L. Rapetti, D. Ferigo, F. J. A. Chavez, and D. Pucci, "Whole-Body Geometric Retargeting for Humanoid Robots," *Humanoids*, 2019.
- [34] S. Caron, Q. C. Pham, and Y. Nakamura, "Stability of surface contacts for humanoid robots: Closed-form formulae of the Contact Wrench Cone for rectangular support areas," *Proceedings - IEEE International Conference on Robotics and Automation*, vol. 2015-June, no. June, pp. 5107–5112, 6 2015.
- [35] J. T. Betts, *Practical Methods for Optimal Control and Estimation Using Nonlinear Programming*. Society for Industrial and Applied Mathematics, 1 2010.
- [36] D. Q. Mayne and H. Michalska, "Receding horizon control of nonlinear systems," *IEEE Transactions on Automatic Control*, vol. 35, no. 7, pp. 814–824, 1990.
- [37] M. Vukobratović, B. Borovac, M. Vukobratov, and B. Borovac, "Zero - Moment Point — Thirty Five Years of Its Life," *International Journal of Humanoid Robotics*, vol. 1, no. 1, pp. 157–173, 2004.
- [38] D. Roetenberg, H. Luinge, and P. Slycke, "Xsens MVN: Full 6DOF Human Motion Tracking Using Miniature Inertial Sensors," p. 9, 2013.
- [39] A. Paszke, S. Gross, F. Massa, A. Lerer, J. Bradbury, G. Chanan, T. Killeen, Z. Lin, N. Gimelshein, L. Antiga, A. Desmaison, A. Kopf, E. Yang, Z. DeVito, M. Raison, A. Tejani, S. Chilamkurthy, B. Steiner, L. Fang, J. Bai, and S. Chintala, "PyTorch: An Imperative Style, High-Performance Deep Learning Library," in *Advances in Neural Information Processing Systems*, vol. 32. Curran Associates, Inc., 2019.
- [40] I. Loshchilov and F. Hutter, "Fixing Weight Decay Regularization in Adam," *CoRR*, vol. abs/1711.05101, 2017.
- [41] O. R. developers, "ONNX Runtime," 2021, version: 1.14.1.
- [42] J. A. E. Andersson, J. Gillis, G. Horn, J. B. Rawlings, and M. Diehl, "CasADi: a software framework for nonlinear optimization and optimal control," *Mathematical Programming Computation* 2018 11:1, vol. 11, no. 1, pp. 1–36, 7 2018.
- [43] A. Wächter and L. T. Biegler, "On the implementation of an interior-point filter line-search algorithm for large-scale nonlinear programming," *Mathematical Programming*, vol. 106, no. 1, pp. 25–57, 3 2006.
- [44] J. Hogg and J. A. Scott, "HSL_MA97 : a bit-compatible multifrontal code for sparse symmetric systems," *Rutherford Appleton Laboratory Technical Reports*, 2011.
- [45] B. Stellato, G. Banjac, P. Goulart, A. Bemporad, and S. Boyd, "OSQP: An Operator Splitting Solver for Quadratic Programs," *2018 UKACC 12th International Conference on Control, CONTROL 2018*, p. 339, 10 2018.
- [46] A. F. Gad, "PyGAD: an intuitive genetic algorithm Python library," *Multimedia Tools and Applications*, vol. 83, no. 20, pp. 58 029–58 042, 12 2023.
- [47] F. Nori, S. Traversaro, J. Eljaik, F. Romano, A. Del Prete, and D. Pucci, "iCub Whole-Body Control through Force Regulation on Rigid Non-Coplanar Contacts," *Frontiers in Robotics and AI*, vol. 2, 2015.